Korean J. Chem. Eng., 36(8), 1226-1234 (2019)
DOI: 10.1007/s11814-019-0301-3

pISSN: 0256-1115
eISSN: 1975-7220

Hydrodesulfurization via heat exchanger network synthesis for ultra-low-sulfur diesel

Hyun-Wook Ryu*, Nam-Geun Kim*, Sung-Oh Kang**, Min Oh***,†, and Chang-Ha Lee*,**,†**

*Graduate School of Integrated Engineering, Yonsei University, 50 Yonsei-ro, Seodaemun-gu, Seoul 03722, Korea
**Department of Chemical and Biomolecular Engineering, Yonsei University,
50 Yonsei-ro, Seodaemun-gu, Seoul 03722, Korea
***Department of Chemical and Biological Engineering, Hanbat National University,
125 Dongseo-daero, Yuseong-gu, Daejeon 34158, Korea
****DOFTECH Corp, 301, 83, Baekbeom-ro 1-gil, Mapo-gu, Seoul 04104, Korea
(*Received 24 January 2019 • accepted 20 May 2019*)

Abstract−In recent decades, the oil refining industry's interest has been geared toward the production of clean fuels that contain fewer impurities such as sulfur and nitrogen compounds. Diesel hydrodesulfurization (DHDS) employed in light gas oil production has been widely applied to remove various impurities such as sulfur, nitrogen, and metal-organic compounds. In this study, the hydrodesulfurization process for the production of ultra-low sulfur diesel was simulated using the Aspen HYSYS hydroprocessing bed module. Then, exergy analysis was conducted. Since the exergy analysis indicated possible energy savings on the conventional DHDS, heat exchanger network (HEN) synthesis was applied to the process. By replacing the heater and cooler with two heat exchangers, 5% of utility energy could be saved compared to the conventional process. Since the modification was relatively simple, the developed HEN synthesis is feasible in the present DHDS.

Keywords: Hydrodesulfurization Process, Ultra-low-sulfur Diesel, Exergy Analysis, Heat Exchanger Network

INTRODUCTION

In recent decades, the oil refining industry has become interested in producing clean fuels that contain lower levels of pollutants such as sulfur, nitrogen, and aromatics [1]. In particular, many countries are implementing tighter environmental regulations on the sulfur content of fuels to reduce the emissions of harmful substances and improve air quality. After 2020, The International Maritime Organization has announced an international environmental regulation for the reduction of the sulfur content of ship oil from the current level of 3.5% to 0.5%. Therefore, the role of sulfur processing processes such as diesel hydrodesulfurization (DHDS) in the refining industry becomes more important [2].

Several studies have been conducted on hydroprocessing equipment and device modeling for hydrodesulfurization (HDS) design based on industrial data using commercial simulators [3]. A lumped parameter dynamic model was developed for the hydrotreating unit of industrial vacuum gas oil and can be applied to demonstrate the tangible economic benefit of improving the operation of the hydrotreater [4]. Hydrotreating unit for gas oil and vacuum gas oil was simulated using the Petro-SIM^{TM} software based on the actual process data [5]. Modeling of industrial Penex isomerization was performed using the Aspen HYSYS petroleum refining isomerization reactor model [6]. The hydrogenation of industrial cocker complex was analyzed, and the optimum operational parameters were suggested [1]. The fixed bed reactor model using four new kinetic lumping approaches was developed for coal tar hydrogenation and the simulated results were verified using the experimental results [7].

Trickle bed reactors (TBR) are widely used in hydrotreating. In general, hydrogen and hydrocarbons concurrently flow downward over a catalytic bed. Since the kinetics and thermodynamics of most reactions improve with temperature, the TBRs are adiabatically operated at high temperatures to enhance hydrotreating performance. To demonstrate the effect of sulfidation on the performance of the catalyst, oxidic unsupported Ni Mo-W catalysts were studied [8]. Moreover, according to a study of the counter-current operation for HDS in TBR, the counter-current operation is superior to the co-current operation in organic sulfur conversion when deep desulfurization is required [9].

In addition to the analysis of reactor performance, energy analysis of the overall process is required to improve the operational efficiency and profit. Exergy analysis is widely used for analyzing and optimizing energy systems because it can identify system inefficiency through quantitative analysis of energy [10]. Through the exergy analysis of shale oil hydrogenation, not only exergy destruction but also optimal operating parameters were suggested for the process [11]. The simulation and exergy analysis for the North Sea oil gas platform using Aspen Plus indicated that the process was thermodynamically needed for further improvement of the efficiency [12].

To improve the energy efficiency of the process, several studies on process integration have been carried out. A representative technology for energy efficient process integration is the heat-exchanger network (HEN) synthesis. The HEN synthesis based on pinch tech-

†To whom correspondence should be addressed.
E-mail: minoh@hanbat.ac.kr, leech@yonsei.ac.kr

nology saved 4.5 MW utility energy at the Skoghall Mill plant [13]. The HEN synthesis for nitric acid production in a petrochemical complex suggested the change of ΔT_{min} from 38 °C to 10 °C to increase heat recovery and reduce utility usage [14].

Although there are many studies on hydrogen processes in the petrochemical industry, only a few studies on the overall integrated process, especially the ultra-low-sulfur diesel (ULSD) hydrotreating process, have been reported. Furthermore, little attention has been paid to the modeling and optimization of the process. In this study, we simulated DHDS for the production of ULSD using the Aspen HYSYS hydroprocessing bed module. The optimal feed for the DHDS was studied by comparing the process efficiencies using various feeds with respect to the analysis of profitability. In addition, since the exergy analysis for the process that uses the optimal feed indicated the need for further process improvement, HEN synthesis was applied to the process that uses the optimal feed and the energy efficiency was compared with that in the conventional DHDS.

PROCESS DESCRIPTION

1. Hydrodesulfurization

The entire DHDS process flow diagram simulated in this study is presented in Fig. 1. The feed preheated by mixing with hydrogen is supplied to the catalyst fixed bed reactor. Sulfur compounds in the feed are converted to H_2S and nitrogen compounds are converted to NH_3. Unsaturated hydrocarbons are also transformed into saturated hydrocarbons. The effluent stream from the reactor is cooled by an air cooler and then separated into a hydrogen-rich gas and a liquid in a separator. In the separated liquid, dissolved H_2S is removed with gases from the diesel stripper and the by-product (light distillate) through the diesel stripper overhead. The desulfurized product is produced from the reactor bottom. Then, H_2S in the effluent gas is removed from an amine unit and the treated gas is utilized as a fuel.

2. Chemical Reactions

The HDS reaction involving organic sulfur compounds is essentially irreversible under industrially applied reaction conditions. A catalytic chemical reaction kinetics in the HDS reaction is limited by the removal of sulfur (S) from refined petroleum products such as natural gas, gasoline, aviation oil, kerosene, and diesel. The hydrodenitrogenation (HDN) reaction is similar to the HDS reaction in which nitrogen compounds react with hydrogen to form NH_3. Typical HDS and HDN reactions in a hydrotreating reactor can be presented as follows:

$$\text{“[R-S]”}+H_2 \xrightarrow[300\text{-}450\,^{\circ}\text{C}]{Catalyst} \text{“[R-S]”}+H_2S \quad (1)$$

$$\text{“[R-N]”}+H_2 \xrightarrow[300\text{-}450\,^{\circ}\text{C}]{Catalyst} \text{“[R-S]”}+NH_3 \quad (2)$$

The hydrodearomatization (HDA) is a reaction in which aromatic compounds and cyclic unsaturated hydrocarbons react with hydrogen to become saturated hydrocarbons.

(3)

The HDS, HDN, and HDA reactions in a TBR occur simultaneously on the catalyst surface and are exothermic. In general, the operating temperature of the HDS reactor is 320-390 °C. To compensate for the gradual deactivation of the catalyst, the operating temperature in a reactor is gradually increased from the start of run to the end of run.

3. EOS and Feed Characterization

Peng-Robinson (PR) and Soave-Redlich-Kwong (SRK) equations of state were used to simulate the DHDS process. The Peng-Robinson (PR) equation of state is suitable for equilibrium prediction of light hydrocarbon mixtures and the Soave-Redlich-Kwong (SRK) equation of state is used to reflect the characteristics of the high-pressure composition and temperature.

Crude oil components can be classified into pseudo-components

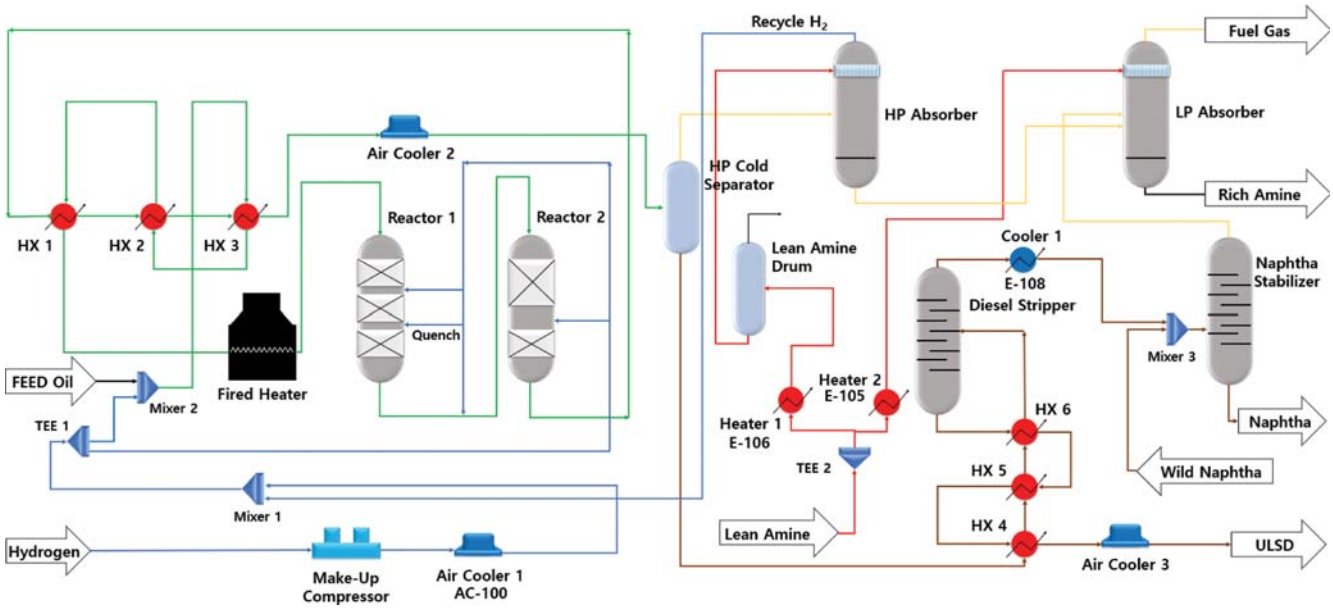

Fig. 1. Schematic of entire DHDS for ULSD.

Table 1. TBP of feed oil information for DHDS simulation

Volume %	TBP °C	Sp. Gravity	API_60	Molecular weight	Liquid density kg m^{-3}
0	75.00	0.70	70.08	68.33	700.55
10	169.07	0.79	48.59	138.71	784.14
20	233.59	0.82	40.57	184.34	820.67
30	244.25	0.83	39.42	193.60	826.21
40	253.42	0.83	38.42	204.92	831.05
60	286.91	0.85	34.97	231.66	848.27
80	330.48	0.87	30.86	274.82	869.75
90	357.29	0.88	28.52	301.54	882.51
95	389.24	0.90	25.90	336.11	897.19
100	423.92	0.91	23.25	380.70	912.57

Table 2. Oil assay characterization for DHDS simulation

Property	Values
Specific gravity	0.83
Sulfur content [wt%]	1.0
Nitrogen content [ppm]	400
Cetane number	49
C to H ratio [wt%]	7.1

Table 3. Feedstock information

Index	Petroleum cut range °C	Composition
1*	59-97	0.062
2*	97-136	0.052
3*	136-174	0.046
4*	174-213	0.051
5*	213-251	0.096
6*	251-289	0.323
7*	289-328	0.132
8*	328-366	0.156
9*	366-405	0.046
10*	405-443	0.036

according to specific gravity, molecular weight, liquid density, or true boiling point (TBP) data. TBP refers to the steam temperature at the time of infinite reflux by condensing the vapor generated by heating the liquid phase at atmospheric pressure when a large number of components such as crude oil and petroleum oil are mixed. Therefore, TBP is expressed by vol%, which is the cumulative volume sequentially separated by temperature. The feed characterization for DHDS simulation, which was obtained from the TBP curve calculated from the Aspen HYSYS petroleum assays module, is shown in Tables 1 and 2.

Feed distillation index (from 1^* to 10^*) is defined as pseudo-components in DHDS. The mixed oil feeds into the process at 40 °C, 130.1 kg_f cm^{-2}, and 224,996 kg h^{-1}. The information on oil feedstock

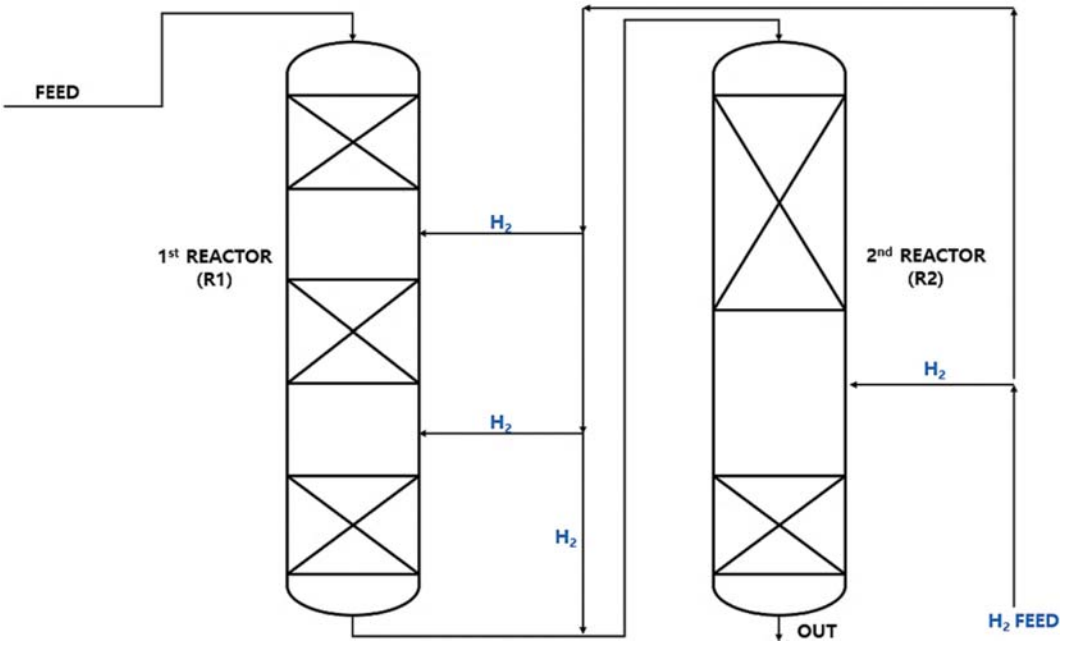

Fig. 2. Schematics of hydrotreating bed reactor.

and petroleum cut point is presented in Table 3.

REACTOR MODEL

1. Operating Conditions of TBR Design

The schematic of the hydrotreating bed reactor is presented in Fig. 2. The first reactor consists of three fixed beds and the second reactor consists of two fixed beds. The TBR is adiabatic and the feed flows into the reactor at 335.9 °C, 118.1 $kg_f\ cm^{-2}$ and 253,095 kg h^{-1}. Alumina-based Co-Mo and Ni-Co-Mo or Ni-Mo catalysts are used to remove sulfur during hydrogenation. The density of the catalyst is in the range of 480-800 kg m^{-3} [16]. The input data of the fixed reactors for the simulation are shown in Table 4.

2. Solution Strategy for Reaction Kinetics

Aspen HYSYS v.10 was used to simulate the hydrotreating TBR. It contains a detailed kinetic model of hydrotreating reactions. The TBR models include reaction rate expressions for HDS, HDN, saturation, cracking, and ring opening. The reactions other than the HDA reactions are irreversible. The reaction network embedded in the hydroprocessor bed has 97 kinetic lumps and 177 reactions. Each reaction is described in terms the Langmuir-Hinshelwood-Hougen-Watson mechanism as shown as (4).

$$\text{Reaction Rate}=\text{Global Activity} * \text{Reaction Class Activity} * \text{Heterogeneous Reaction Rate} \quad (4)$$

Global activity means the overall reaction activity of TBR, and the reaction class activity means the activity for a specific reaction (HDS, HDN). Global activity parameter influences the rate of all reactions [1,6].

Table 4. Input data for TBR simulation

Parameter	Reactor 1			Reactor 2	
Bed	1st	2nd	3rd	1st	2nd
Diameter (m)	3.5			3.5	
Catalyst (kg)	34,000			51,000	68,000
Voidage	0.3				
Density (kg/m^3)	740				

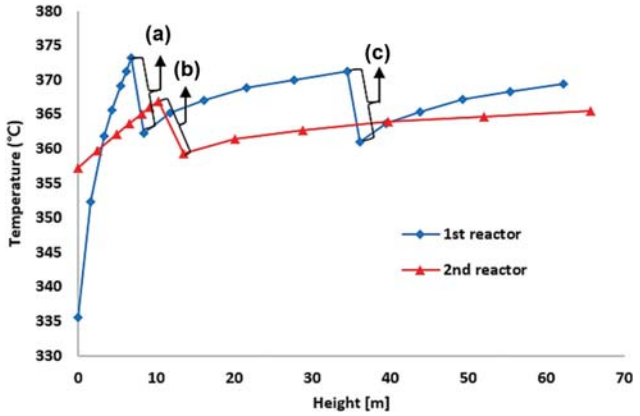

Fig. 3. Operating temperature profiles along TBR height ((a) 7 m-8.5 m, (b) 10 m-13 m, (c) 35 m-36 m).

SIMULATION AND RESULTS

1. Temperature Profile Results in Reactor

The operating temperature profile of the reactor is presented in Fig. 3. The total height of the first reactor is 62 m and the height of the second reactor is 65 m. The temperature in the first reactor dropped rapidly at section "a", which is height of reactor between 7 m and 8.5 m (373 °C to 362 °C), and section "c", which is height of reactor between 35 m and 36 m (371 °C to 361 °C). The temperature in the second reactor dropped speedily at section "b", which is height of reactor between 10 m and 13 m (367 °C to 359 °C). Since the hydrogenation reaction is exothermic, the temperature required for the reaction should be maintained by utilizing the low-temperature hydrogen quench stream between the beds.

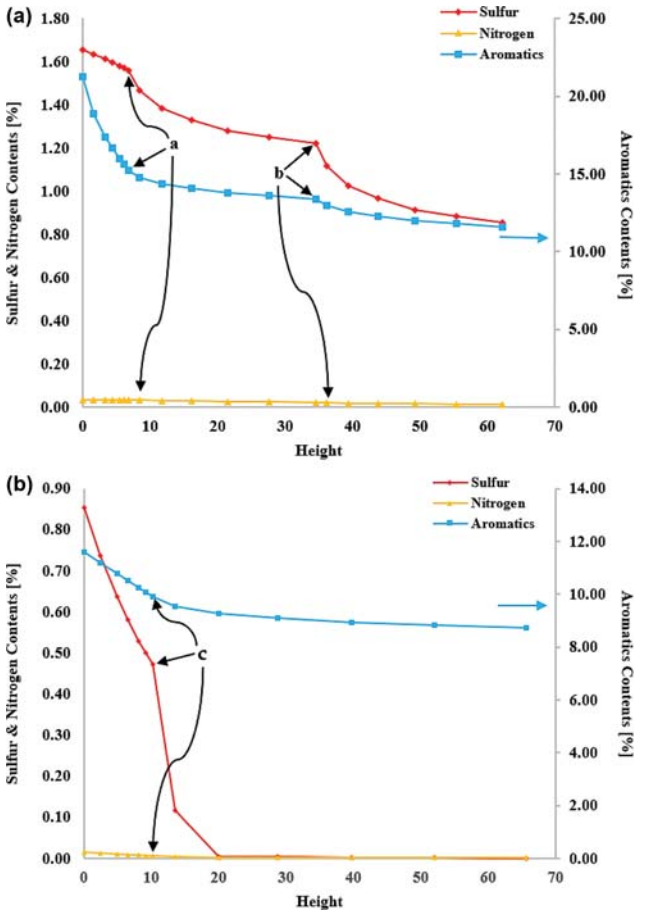

Fig. 4. Concentration profiles of sulfur, nitrogen and aromatics in (a) 1st reactor and (b) 2nd reactor along the TBR height.

Table 5. Elimination % of sulfur and nitrogen in the TBR

TBR			S [wt%] removal	N_2 [wt%] removal
R1	1st	Bed outlet	5.50	0.03
	2nd	Bed outlet	21.77	31.63
	3rd	Bed outlet	30.46	38.61
R2	1st	Bed outlet	44.77	52.93
	2nd	Bed outlet	99.81	79.21

2. HDS, HDN, and HDA Reactions

Figs. 4 (a) and (b) show the simulated concentration profiles for HDS, HDN, and HDA in the first and second reactors. The inflection points at points "a", "b", and "c" are the same as the quenching points at the temperature profile (Fig. 3). The inflection point in the reaction is the point where the low temperature hydrogen is sup-

Table 6. Heat and material balance

Stream name	FEED	H_2 Make-up	LGO	Naphtha
Vapor/Phase fraction	0.00	1.00	0.00	1.00
Temperature [°C]	40.00	40.00	40.00	41.07
Pressure [kg cm^{-2}]	130.10	21.00	9.38	5.67
Mass flow [kg h^{-1}]	224996	3013.31	213756	5446.03
Liq. vol flow [m^3 h^{-1}]	265.90	77.37	259.20	7.41
Comp. weight rates [kg h^{-1}]				
Hydrogen	0.00	2897.49	0.00	0.00
Methane	0.00	115.83	0.00	0.00
1* 59-97*	5617.01	0.00	0.00	0.00
2* 97-136*	5790.88	0.00	0.00	0.00
3* 136-174*	6156.33	0.00	0.00	0.00
4* 174-213*	8168.56	0.00	0.00	0.00
5* 213-251*	18406.6	0.00	0.00	0.00
6* 251-289*	70204.3	0.00	0.00	0.00
7* 289-328*	34435.0	0.00	0.00	0.00
8* 328-366*	46369.4	0.00	0.00	0.00
9* 366-405*	15777.2	0.00	0.00	0.00
10* 405-443*	14071.0	0.00	0.00	0.00
PROD NAP 28-45*	0.00	0.00	0.00	0.00
PROD NAP 45-55*	0.00	0.00	0.00	0.00
PROD NAP 55-65*	0.00	0.00	0.00	98.34
PROD NAP 65-75*	0.00	0.00	0.91	2019.81
PROD NAP 75-85*	0.00	0.00	8.15	748.51
PROD NAP 85-100*	0.00	0.00	1075.67	1338.07
PROD NAP 100-115*	0.00	0.00	2370.90	44.82
PROD NAP 115-125*	0.00	0.00	4071.86	5.36
PROD DSL 125-140*	0.00	0.00	2401.67	0.27
PROD DSL 140-155*	0.00	0.00	2381.85	0.01
PROD DSL 155-170*	0.00	0.00	1657.76	0.00
PROD DSL 170-200*	0.00	0.00	6342.99	0.00
PROD DSL 200-230*	0.00	0.00	35837.1	0.00
PROD DSL 230-260*	0.00	0.00	12318.4	0.00
PROD DSL 260-290*	0.00	0.00	39120.1	0.00
PROD DSL 290-320*	0.00	0.00	30948.0	0.00
PROD DSL 320-350*	0.00	0.00	46438.5	0.00
PROD DSL 350-380*	0.00	0.00	15511.5	0.00
PROD DSL 380-410*	0.00	0.00	8732.14	0.00
PROD DSL 410-443*	0.00	0.00	4538.64	0.00
DN 28-60*	0.00	0.00	0.000	124.18
DN 60-90*	0.00	0.00	0.000	132.64
DN 90-122*	0.00	0.00	0.000	137.79
DN 122-138*	0.00	0.00	0.000	278.46
DN 138-150*	0.00	0.00	0.000	261.22
DN 150-167*	0.00	0.00	0.000	184.23
DN 167-185*	0.00	0.00	0.000	58.00
DN 185-204*	0.00	0.00	0.000	12.61
DN 204-227*	0.00	0.00	0.000	1.73

plied for quenching.

In the first reactor, the amount of nitrogen compounds and unsaturated hydrocarbon was significantly reduced compared to sulfur compounds. In the second reactor, the amount of both sulfur and nitrogen compounds was steeply reduced, while the conversion of unsaturated hydrocarbons was relatively small. The variations in sulfur and nitrogen levels in both reactors were similar because these compounds were affected by the catalyst activities [17,18]. The final product contained a negligible amount of sulfur content. Table 5 presents the removal efficiency of sulfur and nitrogen in the oil treated from the TBR.

Generally, steep changes (abrupt increase in conversion) occur in early part of the reactor. According to the concentration profiles at Fig. 4, the sulfur and nitrogen concentration in the first Bed reactor (Height from 0 to a, Fig. 4(a)) decreased gradually. It is inferred that the reaction quotient for HDS and HDN at the first bed in the reactor was somewhat affected by the catalyst, consequently affecting the rates for HDS and HDN. Thus, HDS and HDN reaction rate was dependent on the temperature, space velocity, hydrogen partial pressure and catalyst type. Most HDS and HDN reactions are straightforward except those of aromatic sulfur, and nitrogen species (Benzothiophene, Quinoline etc.), which starts with ring opening sulfur and nitrogen removal, followed by saturation of the resulting olefin. The maximum aromatic reduction is a function of the type and amount of aromatic compounds in the feed.

Table 6 summarizes the simulation results on the heat and material balance (HMB). In Table 6, DSL and NAP indicate desulfurized LGO and naphtha. DN is the wild naphtha from the other processes. According to the simulation results, ULSD with 0.001 wt% of sulfur and 14.52 ppmwt of nitrogen can be produced at a rate of 14,289,439 bbl yr^{-1}.

PARAMETRIC STUDY

1. Exergy Analysis of DHDS in Conventional Case

Exergy is the theoretically obtainable maximum work when a system is in equilibrium and can be expressed using Eq. (5):

$$\text{Exergy} = E^{kn} + E^{pt} + E^{ch} + E^{ph} \tag{5}$$

where E^{kn} is the kinetic exergy. Kinetic exergy is mostly pertinent where speeds are significant, which is like in a turbine and the kinetic exergy can be expressed using Eq. (6):

$$E^{kn} = ke = \frac{V^2}{2} \tag{6}$$

E^{pt} is the exergy from potential exergy. Potential exergy used to be pertinent for electrical or hydraulic systems and potential exergy can be expressed using Eq. (7):

$$E^{pt} = pe = gz \tag{7}$$

Generally, kinetic and potential exergy terms can be ignored in the industrial processes. E^{ch} is the chemical exergy caused by the reaction and it is applicable for the chemical energy of a fuel is converted to electricity via a chemical reaction, biomass gasification equipment and petrochemical processing plant. Chemical exergy is expressed as follows Eq. (8):

$$E^{ch} = \overline{R}T_0 \sum_i y_{i,0} \ln\left(\frac{y_{i,0}}{y_{i,0,0}}\right) \tag{8}$$

E^{ph} is the physical exergy due to the difference in temperature and pressure for a reference state.

Physical exergy is expressed as follows:

$$E^{ph} = (H - H_0) - T_0(S - S_0) \tag{9}$$

Here, the subscript "0" shows the reference state for calculating the exergy in terms of thermal and mechanical equilibrium. According to Eq. (9), physical exergy is the work done by the relative change in temperature and pressure in the system. In this study, chemical, potential and kinetic exergies were neglected [15]. Exergy analysis was performed in terms of the physical exergy on streams only. The results showed that 63.3% of total exergy destruction in DHDS occurred in the cooler, heat exchanger, and the heater. In addition, exergy destruction was higher in the mixer, the tower (naphtha stabilizer and diesel stripper and low-pressure absorber), and the vessel, in that order. Exergy destruction occurred mainly in the control volume due to the increase or decrease in external temperature by friction loss. Since loss and destruction are irreversible in the system [16], irreversibility can occur in mixing, chemical reactions, and heat transfer including friction. In the simulation, total exergy destruction in the DHDS was 118.12 MW.

Fig. 5 shows the exergy destruction ratio in the DHDS. The exergy destruction at the cooler and the heater stemmed from the temperature differences in the process and the utility. Since the heat exchanger also caused significant exergy destruction, it was recommended to be improved by the pinch technology or the HEN synthesis. Exergy destruction in the mixer was mainly caused by the temperature difference between the fluids from the process streams. It is concluded that the higher the temperature difference causes the larger the exergy destruction.

2. Heat-exchanger Network Synthesis in Conventional Case

Heat exchanger network (HEN) synthesis is an extensively studied design problem in chemical engineering. The objective of HEN synthesis is to achieve the target temperature when there are "m" cold streams to be heated from the supply temperature T_{sc} (Temperature of supply cold stream) to the target temperature T_{tc} (Temperature of target cold stream) and "n" hot streams to be cooled from the supply temperature T_{sh} (Temperature of supply hot stream) to the target temperature T_{th} (Temperature of target hot stream).

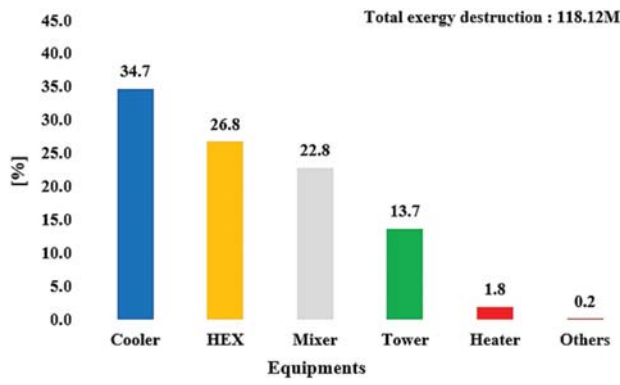

Fig. 5. Exergy destruction ratio in DHDS.

The configuration of this HEN synthesis in simulation is local optimization.

According to the exergy analysis, the energy efficiency of the process can be improved by developing a modified process configuration for the heat exchanger, cooler, and the heater. In this study, the HEN synthesis was performed to reduce the utility energy in the entire process. In the shell & tube heat exchanger, ΔT_{min} is recommended at 20-40 °C for oil refining, 10-20 °C for petrochemical and chemical processes, and 3-5 °C for low-temperature processes [20]. The pinch approach temperature for the simulation was set at 30 °C. The HEN synthesis in the study is shown in Fig. 6.

With reference to the integration between air cooler-100 and preheater E-106 of HX-105. the hot fluid outlet temperature was calculated to be 115 °C (After synthesis to Mixer-1 stream) when the outlet temperature of the cold stream was set at 61 °C (After synthesis to C-103 (LP Absorber) stream). Although this was higher than the target temperature of 60 °C (Before synthesis To Mixer-1 stream), this discrepancy did not affect the overall process since the stream temperature was reduced by mixing it with a cold hydrogen stream for the hydrodesulfurization. Therefore, after integration of cooler and preheater, the performance of entire process was not influenced by the integration of heaters and coolers. Detailed comparison between the heat exchanger streams before and after the integration is shown in Table 7.

Two heat exchangers added for the HEN synthesis follow a thermal model as shown in Eq. (10).

$$Q = \dot{m} C_p \Delta T \tag{10}$$

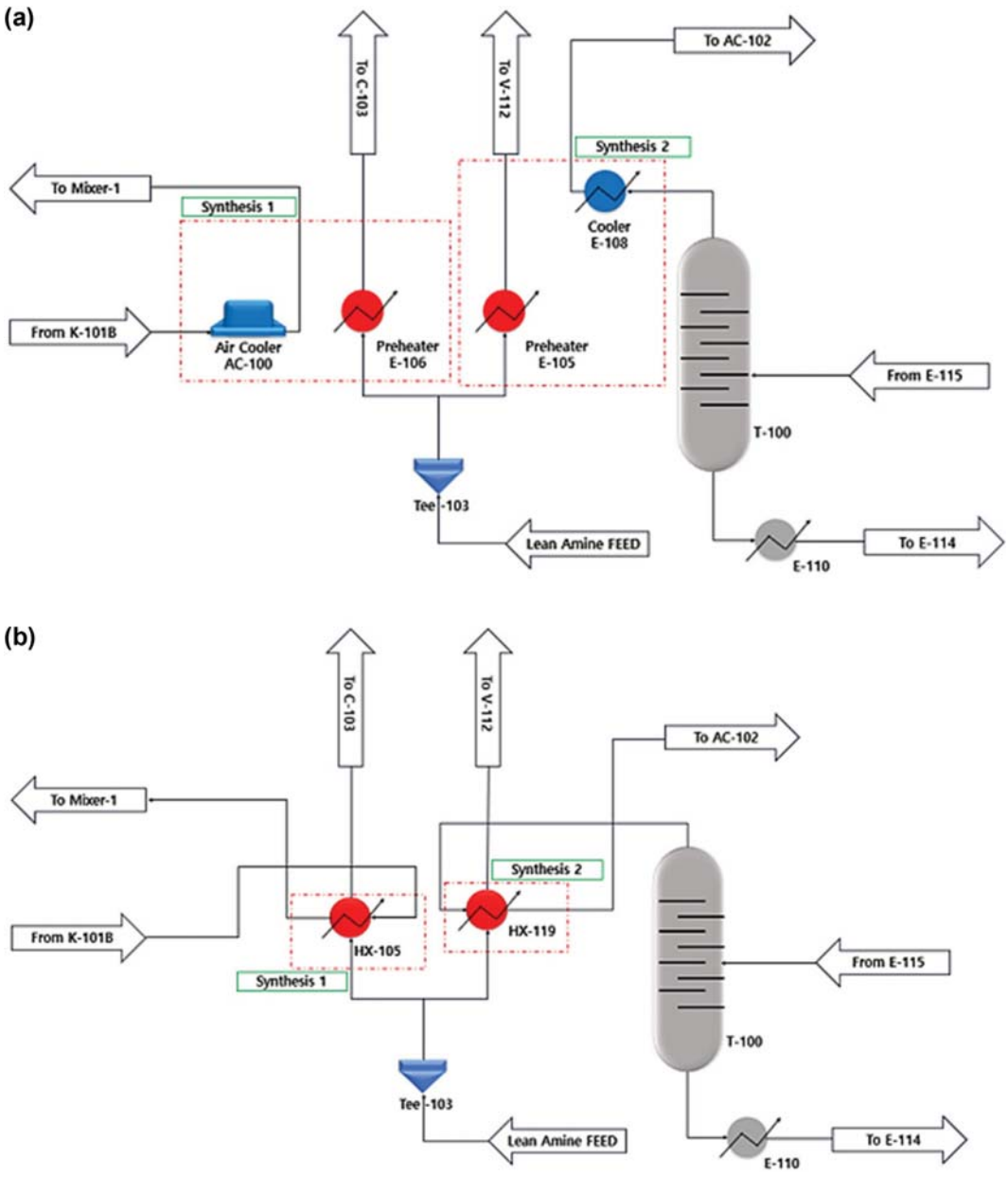

Fig. 6. HEN synthesis: (a) the cooler and heater in conventional PFD and (b) the heat exchangers in modified PFD.

Table 7. Before and after integration on synthesis

Before synthesis	From K-101B	Recycle H_2	To Mixer-1	*To process	From Tee-103	To C-103
Temperature [°C]	172.37	59.32	60.00	59.37	40.00	61.70
Pressure [kg/cm^2]	105.74	103.6	105.74	103.60	9.70	5.90
Molar flow [kgmole/hr]	1444.55	15081.38	1444.55	16525.93	1422.00	1422.00
Mass flow [kg/hr]	3013.31	49021.19	3013.31	52034.50	29872.79	29872.79
After synthesis	From K-101B	Recycle H_2	To Mixer-1	*To process	From Tee-103	To C-103
Temperature [°C]	172.37	58.41	115.51	63.29	40.00	61.00
Pressure [kg/cm^2]	105.74	103.60	105.74	103.60	9.70	5.83
Molar flow [kgmole/hr]	1444.55	15211.45	1444.55	16656.00	1422.00	1422.00
Mass flow [kg/hr]	3013.31	49691.16	3013.31	52704.47	29872.79	29872.79

The heat transfer area of the heat exchanger is modeled as Eq. (11).

$$\text{Area} = \frac{Q}{U \times \Delta T_{LMTD}} \tag{11}$$

The calculation of the investment cost associated with each HEN synthesis is defined by Eq. (12). The heat exchanger was set to the shell and tube type, which is widely used in the industry. In CAPEX of heat exchanger, "a" is the installation cost, "b" and "c" are the duty/area-related to cost set coefficient. N_{shell} is the number of heat exchanger shells [3].

$$\text{CAPEX} = a + b\left(\frac{\text{Area}}{N_{shell}}\right)^{c} N_{shell} \tag{12}$$

The resultant process flow diagram of DHDS modified by the HEN synthesis at heat exchanger (a) and (b) is presented in Fig. 7. Compared with Fig. 1, the process modification was not significant. It is more realistic in industrial fields because the modification of conventional DHDS is practically difficult. Fig. 8 shows the changes in utility energy after the HEN synthesis. According to the results of the HEN synthesis using the energy analyzer, 5% of total utility energy (101.2 MW of 106.1 MW of the conventional process) could be saved. The relative reduction was higher in heat utilities than in cold utilities. However, the absolute value of the saved energy was almost the same in both utilities.

The expected accuracy range of the cost was Class 3 (10-30%) accuracy compared to the prices of the real industry. The capital costs of two additional heat exchangers were \$782,106 and \$791,246. The payback period was calculated by dividing the extra capital cost by energy saving cost/yr [3]. The payback periods for each heat exchanger were 1.0 and 1.3 yr, respectively, because annual energy cost savings were \$746,906 yr^{-1} and \$575,263 yr^{-1} at both exchangers. The results indicate that the conventional DHDS is well

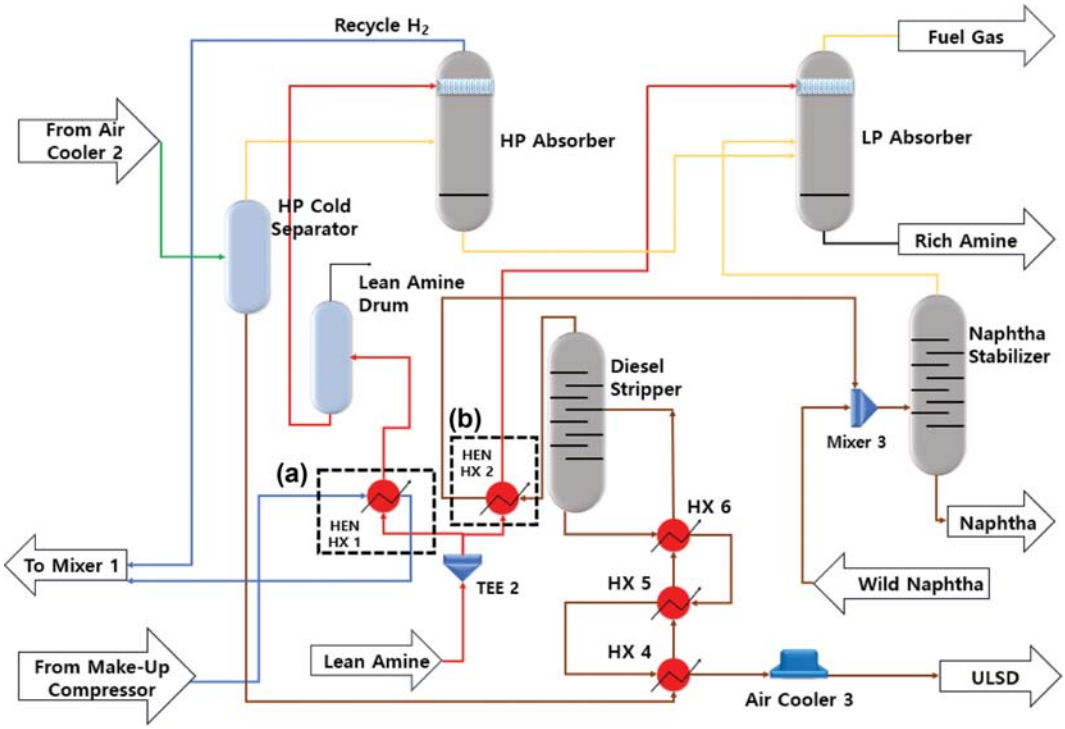

Fig. 7. HEN synthesis at heat exchanger (a) and (b) points in DHDS for ULSD.

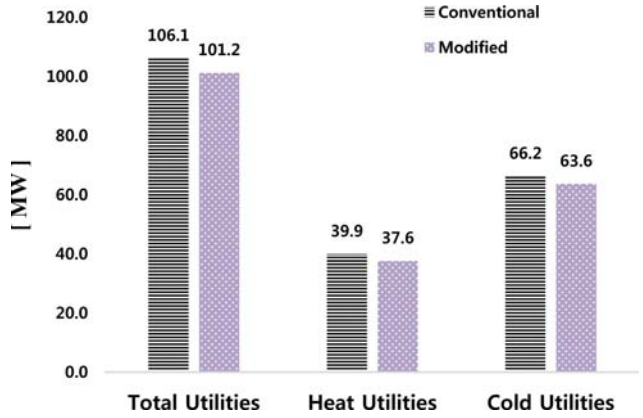

Fig. 8. Comparison of utility energy between conventional and modified processes.

designed, but energy savings are possible by feasible modification even though the savings level is not high.

CONCLUSION

DHDS for ULSD production was simulated and exergy analysis was conducted. The exergy analysis suggested the need for process improvement in the conventional process, especially in the heat exchanger, cooler, and the heater. To reduce energy consumption in the entire process, HEN synthesis was performed to reduce the utility energy of DHDS. Two heaters and coolers were removed from the conventional DHDS and two heat exchangers were added to synthesize the HEN. When the two heat exchangers were added, the extra capital cost was \$782,106 and \$791,246 for each of them. The payback period was 1 yr and 1.3 yr, because annual energy cost savings were \$746,906 yr^{-1} and \$575,263 yr^{-1} from each heat exchanger. The results indicate that 5% energy conservation in the conventional process is feasible through the HEN synthesis. Even though the energy savings is not significant, energy efficiency enhancement is possible with relatively simple modifications. Henceforth, the results can be used as a guideline for process design and energy efficiency for DHDS Process.

ACKNOWLEDGEMENTS

This work was supported by the Industrial Strategic Technology Development Program-Engineering Core Technology Development Project (Project No. 10077467, Development of basic design and FEED automation task support system based on Cloud system) funded by the Ministry of Trade, Industry & Energy (MOTIE, Korea).

REFERENCES

1. E. S. Sbaaei and T. S. Ahmed, *Fuel*, **212**, 61 (2018).
2. "IMO 2020 SOx regulation," Shipping NewsNet.com, last modified n.d., accessed May 15, 2019, http://www.shippingnewsnet.com/news/articleView.html?idxno=24990.
3. Aspen technology, "Aspen Energy Analyzer Reference Guide v10.0" Aspen technology, USA (2018).
4. D. Remesat, B. Young and W. Y. Surcek, *Chem. Eng. Res. Des.*, **87**(2A), 153 (2009).
5. D. Diane, F. R. Maria and Â. Cristina, *Técnico Lisboa.* (2016).
6. M. M. Said, T. S. Ahmed and T. M. Moustafa, *Energy Fuels*, **28**(12), 7726 (2014).
7. F. Dai, H. Y. Wang, M. M. Gong, C. S. Li, Z. X. Li and S. J. Zhang, *Energy Fuels*, **29**(11), 7532 (2015).
8. C. Yin and Y. Wang, *Korean J. Chem. Eng.*, **34**(4), 1004 (2017).
9. H. Yamada and S. Goto, *Korean J. Chem. Eng.*, **21**(4), 773 (2004).
10. M. H. Park, C. Kim and G. Tsatsaronis, *Korean J. Chem.*, **2**, 3557 (1998).
11. X. Luo, Q. Guo, D. Zhang, D. Zhou and Q. Yang, *Appl. Therm. Eng.*, **140**, 102 (2018).
12. T. V. Nguyen, L. Pierobon and B. Elmegaard, *Energy*, **62**, 23 (2013).
13. C. Bengtsson, R. Nordman and T. Berntsson, *Appl. Therm. Eng.*, **22**(9), 1069 (2002).
14. L. J. Matijasevic and H. Otmacic, *Appl. Therm. Eng.*, **22**, 477 (2002).
15. I. Dincer and M. A. Rosen, *Elsevier Sci.*, **2**, 31 (2013).
16. J. Y. Yi and C. Lee, *KSFM*, **18**(6), 19 (2015).
17. D. Bose, *WSN*, **3**, 99 (2015).
18. A. Koriakin, K. M. Ponvel and C. H. Lee, *Chem. Eng. J.*, **162**(2), 649 (2010).
19. J. M. Kwon, J. H. Moon, Y. S. Bae, D. G. Lee, H. C. Sohn and C. H. Lee, *Chem. Sus. Chem.*, **1**, 307 (2008).
20. "Pinch Technology: Basics for the Beginners," http://pages.mtu.edu, last modified n.d., accessed May 15, 2019, http://pages.mtu.edu/~jwsuther/erdm/pinchtech.pdf.